



# X-ray computed tomography to investigate industrial cast Al-alloys

Ajith Bandara<sup>1</sup> · Koichi Kan<sup>1</sup> · Hisashi Morii<sup>2</sup> · Akifumi Koike<sup>2</sup> · Toru Aoki<sup>2,3</sup>

Received: 6 September 2019 / Accepted: 16 December 2019 / Published online: 20 December 2019  
© German Academic Society for Production Engineering (WGP) 2019

## Abstract

This paper describes the use of X-ray computed tomography (XCT) to inspect the internal defects of industrial Aluminum alloys die-casting, to justify the adequateness of super sealant resins in filling tiny holes, and to reduce the casting porosity of metals by the impregnation process. High-resolution 2D slice images were generated by a microfocus X-ray CT system with direct conversion Cadmium Telluride (CdTe) flat panel detector (FPD). Moreover, we were able to visualize the internal defects of the two different shapes of casting objects. The gray-value contrasts of the CT images were excellent to distinguish the resin material in the alloy samples after impregnation treatment. Furthermore, to determine the dimensions of internal defects, virtual sectioning was carried out to view the cross-section of the metal samples and dimensions of internal defects. Dual-energy X-ray computed tomography (DXCT) was used with an energy differentiation type 64-pixel linear array photon-counting line sensor for the material characterization. The impregnated resin part inside the castings defects was verified based on the effective atomic number with a 2.92% low error margin. Hence, this will be a useful qualitative and quantitative advancement to rapid and detailed non-destructive analysis within the die-casting industries in improving the quality of the impregnation process.

**Keywords** X-ray computed tomography (XCT) · Non-destructive analysis · Semiconductor X-ray detectors · Image reconstruction · Al-alloys die-casting · Impregnation

## 1 Introduction

The die-casting process is used to produce geometrically-complex metal parts, using reusable molds for different industrial applications [1]. Aluminum-alloy die-casting is the most widely-used technique for industries, such as automobiles, precious machinery, communication, LED displays, LED lamps, and furniture, and the list goes on [2–4]. The quality of the cast metals is affected by several internal defects, for example, coarse microstructures, pores, oxides, among others [5]. The impregnation technique is used to get rid of these defects and to make metal components reusable [6]. However, evaluating the adequacy of the impregnation

resin inside the casted metals is very important for assessing the quality of the product. Traditional techniques, such as ultrasound and radiographic testing, are used to detect any defects [7], but they are unable to visualize all the internal defects with material identification. Currently, the pressure inspection technique is used to evaluate holes and porosity inside the cast metals, based on the leak rate; however, this method cannot be used to assure the adequacy of impregnation for preserving the quality of the cast metals. Therefore, we have planned to use a microfocus X-ray computed tomography (XCT) technique, with improved performance, in order to visualize and characterize the defects and to analyze the impregnated resin inside the aluminum-alloy cast samples.

XCT has become an advanced technique in both medical and industrial fields for visualizing interior features and material characterization. This nondestructive analysis technique has been practiced in the industrial sector since the early 1990s [8–12]. This powerful technology has great potential in industrial sectors for quality inspection and dimensional metrology applications. Also, the usability of the XCT technique is improving due to the continued

✉ Ajith Bandara  
chuhatsu.gkc1@gmail.com

<sup>1</sup> Hamamatsu TSC, Chuo Hatsumei Institute, 322 Lida-cho, Minami-ku, Hamamatsu 435-0028, Japan

<sup>2</sup> ANSeeN Inc, Johoku 3-5-1, Hamamatsu, Shizuoka 432-8561, Japan

<sup>3</sup> Research Institute of Electronics, Shizuoka University, Johoku 3-5-1, Hamamatsu, Shizuoka 432-8561, Japan

progress of software and hardware development in industrial CT analysis [13]. The penetration ability of high energy radiation such as X-ray and gamma-ray through an object provides the path to visualizing the interior structure of an object without any form of contact. It eliminates the need to cut or destroy the part. It is also possible to perform high accuracy analysis of complex internal geometries that are not possible with any other measurement technology. Primarily, the image quality of the X-ray CT depends on detector performance, and the direct bandgap CdTe semiconductor shows excellent performance as direct conversion X-ray sensors. High-density CdTe compound semiconductor material has great potential to capture X-rays directly to interact with electrons. Hence, this shows higher conversion efficiency than the conversion of X-rays by scintillating. Moreover, a stable crystalline CdTe detector can measure X-ray energy by photon counting. Hence, a dual-energy X-ray computed tomography (DXCT) method [14, 15] can be employed with CdTe photon counting line sensors to materialize discrimination based on linear attenuation coefficient for several energy windows. There have been several studies about XCT of Al-alloys; for example, Kastner et al. [16] published high-resolution cone-beam XCT of 3D microstructures of cast Al-alloys in 2011. Kan et al. [17], in our research group, studied the application of photon-counting XCT to Al-casting inspection in 2013. In recent XCT of Titanium Aerospace, investment casting was studied by du Plessis et al. [18].

In this paper, we successfully describe the use of a semi-automated high-energy microfocus X-ray CT system with a new in-house-developed CdTe Flat Panel Detector (FPD) for the cast Al-alloys inspection. This lightweight, portable, and compact FPD has many advantages such as direct conversion, 100% conversion energy signal, optical diffusion-free imaging, High-speed processing with LSI, and gapless tiling. Typically, it requires several hours to take quality

projection data and detailed analysis. However, with the FPD and our advanced cone-beam CT reconstruction software, high-resolution digital images of thicker or heavier material with detailed analysis could be prepared in several minutes. A higher number of projection images of an object can also be obtained by smoothly controlling the frame rate of the FPD (maximum is 100FPS). The X-ray energy, detector movement, sample holder movement/rotation, and data acquisition time can precisely be controlled with a software system. The impregnated polymer resin (P601) that we synthesized and used in the experiment is also a highly stable new organic impregnant in the Al-alloys die casting. High contrast and spatial resolution CT slice images of the metal samples before and after impregnation treatment was generated. The gray-value contrasts of the defects and the impregnated showed excellent qualitative identification with their dimensions. The DXCT method was used to quantitatively confirm the impregnate resin material inside the internal defects, and also alloy metal parts based on their effective atomic numbers. This research study proved that the high-resolution microfocus CT technique with improved CdTe flat panel detectors, along with the X-ray system with a stage controller, could be efficiently and effectively used for industrial cast alloys inspections and material identifications.

## 2 Experimental section

### 2.1 Samples and impregnation

In this study, two different shapes and dimensions of cast Al-alloys samples were used to investigate the X-ray Computed Tomography technique. Before and after impregnation are shown in Fig. 1. An impregnation process was carried out using a vacuum-dip pressure method with a super seal

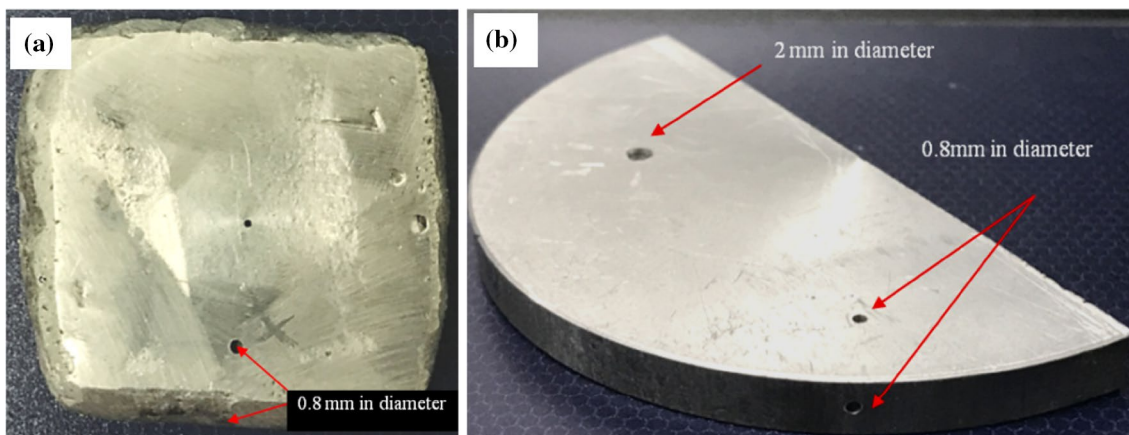


**Fig. 1** Photo images of the Al-alloy test pieces with  $28 \times 28 \times 10 \text{ mm}^3$  cuboid and half circle with 60 mm in diameter and 5 mm in thickness shown in **a** and **b**

P601 polymer compound as the impregnate resin [17]. The commercially used P601 resin solution consists mainly of 2-Hydroxyethyl Methacrylate ( $C_6H_{10}O_3$ ) ester monomer and allows to polymerize during the impregnation process.

The 0.8 mm tiny range holes which we created in perpendicular directions to each other of both cuboid and half-circle alloys test pieces for the impregnation process depicted in Fig. 1a, b.

## 2.2 Characterization methods

There are two steps of the research. First, the qualitative study of the cast alloy samples for interior defect analysis was carried out with the CdTe flat panel detector (ANseeN Inc) and quantitative technique, which uses material identification conducted with photon-counting 64-pixel Linear Array Radiation line sensor (Hamamatsu) using microfocus SMX-150CTS system for X-ray generation. The X-ray source is the same for both of the analyses.

### 2.2.1 Qualitative analysis

CdTe 2D array flat panel detector, which consists of 100  $\mu\text{m}$  size pixels in the 252 rows and 1024 columns, was set up to obtain projection images over  $360^\circ$  of each sample with a cone-beam geometry of SMX-150CTS system as shown below Fig. 2. The distance between the X-ray source and detector was fixed to 600 mm, while the source to sample distance was controlled as 300 mm for cuboid and 500 mm for half circle alloys samples, respectively. A CT scan was carried out for both samples in  $5^\circ/\text{s}$  slow stepwise rotations with 130 kV and 500  $\mu\text{A}$  parameters for X-ray generation.

The detector calibration was conducted before the measurement and projection images of the alloy samples were recorded at a frame rate of 10 and 50, before and after the impregnating treatment, respectively. Then all the 2D projection images were computationally converted to 3D slice images, using the filtered back-projection method [19], and the background noises were removed by applying image filtering.

The sample and detector alignments are significant in the creation of a sharp and accurate CT image. Hence, the mid-point of the sample and detector were carefully aligned during the experimental set-up, and further fine controlling was done using Cone Beam Computed Tomography (CBCT) image reconstruction software. The reconstructed 3D images of the cast alloy samples can be visualized either by CT stacked slices or 3D volume data.

### 2.2.2 Quantitative analysis

Projection radiographs of the cuboid cast Al-alloys sample (after the impregnating treatment) were measured with the 64-pixel linear array photon-counting radiation line sensor over  $360^\circ$  at  $5^\circ/\text{s}$ . The slow, step-wise, rotational scanning of the sample was placed between the X-ray source and the detector, as depicted in Fig. 3 below. In this step, we used a collimator to obtain the fan-beam geometry of the X-ray source with a thickness of several millimeters, and the detector was calibrated for energy response before the data acquisition. The X-ray source was fixed, and the X-ray source-detector distance was approximately 600 mm, and the distance between source-to-sample was 350 mm to achieve higher magnification and, thus, better spatial resolution.

This energy differentiation type CdTe semiconductor detector has 64 pixels, arranged in a line array with the size of each pixel being 100  $\mu\text{m}$ . The five comparators differentiate the signal pulses from each detector pixel according to their energy levels. In this instance we have selected 50 keV, 70 keV, 90 keV, 110 keV, and 130 keV as five different energy thresholds to obtain 2D radiographs through the alloy samples and then CT images are reconstructed using the Filtered Back-Projection Technique with 50–90 keV low and 90–130 keV high energy X-ray spectra for material differentiation in DXCT using a formula introduced by Jackson and Hawkes [20, 21]. They have proposed a formula to identify various materials by their effective atomic numbers ( $Z$ ) based on linear attenuation coefficients ( $\mu$ ) of materials at two distinct energy windows ( $E_1$ ,  $E_2$ ) as given in the following formula 1. This method has high accuracy for the

**Fig. 2** Schematic diagram of the experimental setup of the flat panel detector

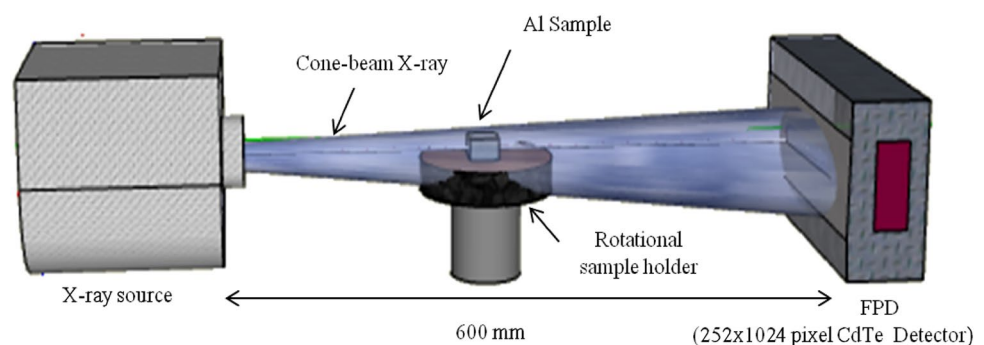
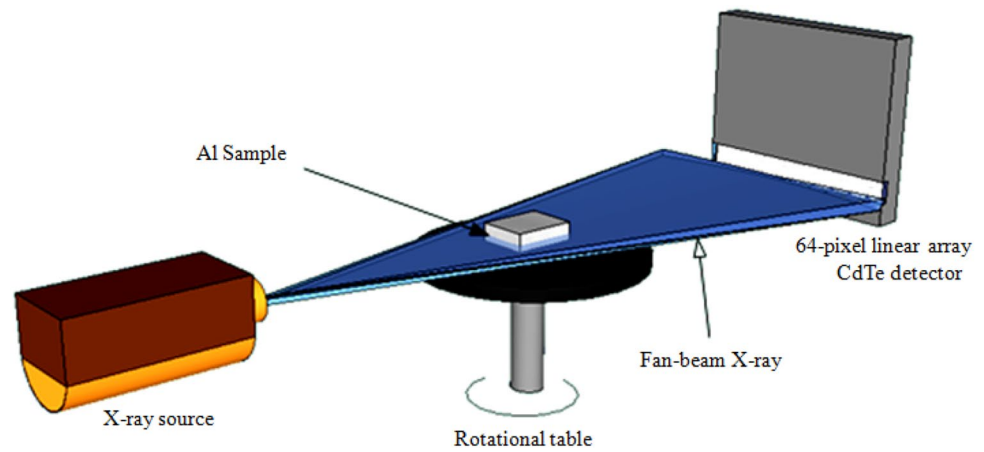


**Fig. 3** Schematic diagram of the experimental setup of a 64-pixel linear array photon-counting detector



attenuation process over an energy range of 30–150 keV and for materials with an atomic number of less than 50 [22].

$$Z^4 = \frac{\mu(E_2)G(E_1, Z) - \mu(E_1)G(E_2, Z)}{\mu(E_1)F(E_2, Z) - \mu(E_2)F(E_1, Z)} \quad (1)$$

where;  $G(E, Z)$  is the electron cross-section according to the scattering term.  $F(E, Z)$  is the photoelectric effect.

### 3 Results and discussion

#### 3.1 Qualitative analysis of the cast Al-alloy samples

The  $252 \times 1024$  pixel CdTe 2D array Flat panel Detector can easily be employed to take high resolution, high speed, and high sensitivity measurements of the cast alloy samples. 2D digital X-ray projection images of both Al samples were recorded before the impregnation process. Then the 3D CT data set was reconstructed from all 2D radiographs around the samples to generate and visualize volume data for further analysis. The Al-alloy test objects can be visualized entirely using reconstructed 3D slice images for detailed internal defect analysis. However, the resolution and detectability of the image are dependent on the focal spot size of the X-ray source, radiation detector, and geometrical magnification of the object.

Some of the high-resolution slice images of both samples under the above experimental conditions are shown in Figs. 4 and 5, respectively. Those images show the internal defects with excellent contrast without destroying the sample. We generated 252 CT slice images computationally in order to view a complete sample of the cast Al-alloys moving from one side to the other across the object, and this does not require any special software for observational purposes.

We have presented only some of the slices in this work. The brighter areas correspond to highly dense metal, while dark areas represent air in the diagrams above. Therefore,

those black spots are voids. The cuboid sample has many defects that might have occurred in the die-casting process as compared to the half-circle cast alloy ones. There are different subclasses of defects that can be identified in the High-Pressure Die-Casting (HPDC) production process. Major die-casting defects are blowhole (circular voids), shrinkage, cold shut, flow line, and misrun. Apart from shrinkage, other artifacts are mainly caused by trapped air during molten metal feeding. Also, the different sizes of voids in the cuboid sample are associated with the amount of trapped air or gases. These defects can be minimized or eliminated by evacuating the air in die cavities. An ultra-high-vacuum die-casting process has been developed and is beginning to be applied to produce high-quality die-casting parts. Although some ring- and beam-hardening artifacts appeared in the images above, they do not affect the defects analysis. However, the quality of the CT images can be improved slightly by proper detector calibration with an advanced filtering technique. These slice images are the straightforward form of CT analysis, and the 3D bulk image has also been presented, as shown in Fig. 6.

The scanning conditions are also vital to the visualization of tiny defects in the material. In this study, the resolution for the cuboid sample was 0.15 mm and 0.26 mm for the half-circle object. The resolution of both samples is the voxel edge length. Therefore, it is unable to detect the defects or features smaller than twice the scan resolution under these experimental conditions, and tiny internal holes which we created on both objects for the impregnation process visualizes with these parameters. However, the detectability and accuracy of the defects would improve further with high scan resolution. Virtual sectioning also applied to 3D CT images of both samples in all the directions for further internal defect analysis using the Osirix software and dimensions of defects of the cuboid cast metal sample illustrated in Fig. 7.

In particular, the above diagrams show dimensions of the two holes which are perpendicular to each other. Figure 7a

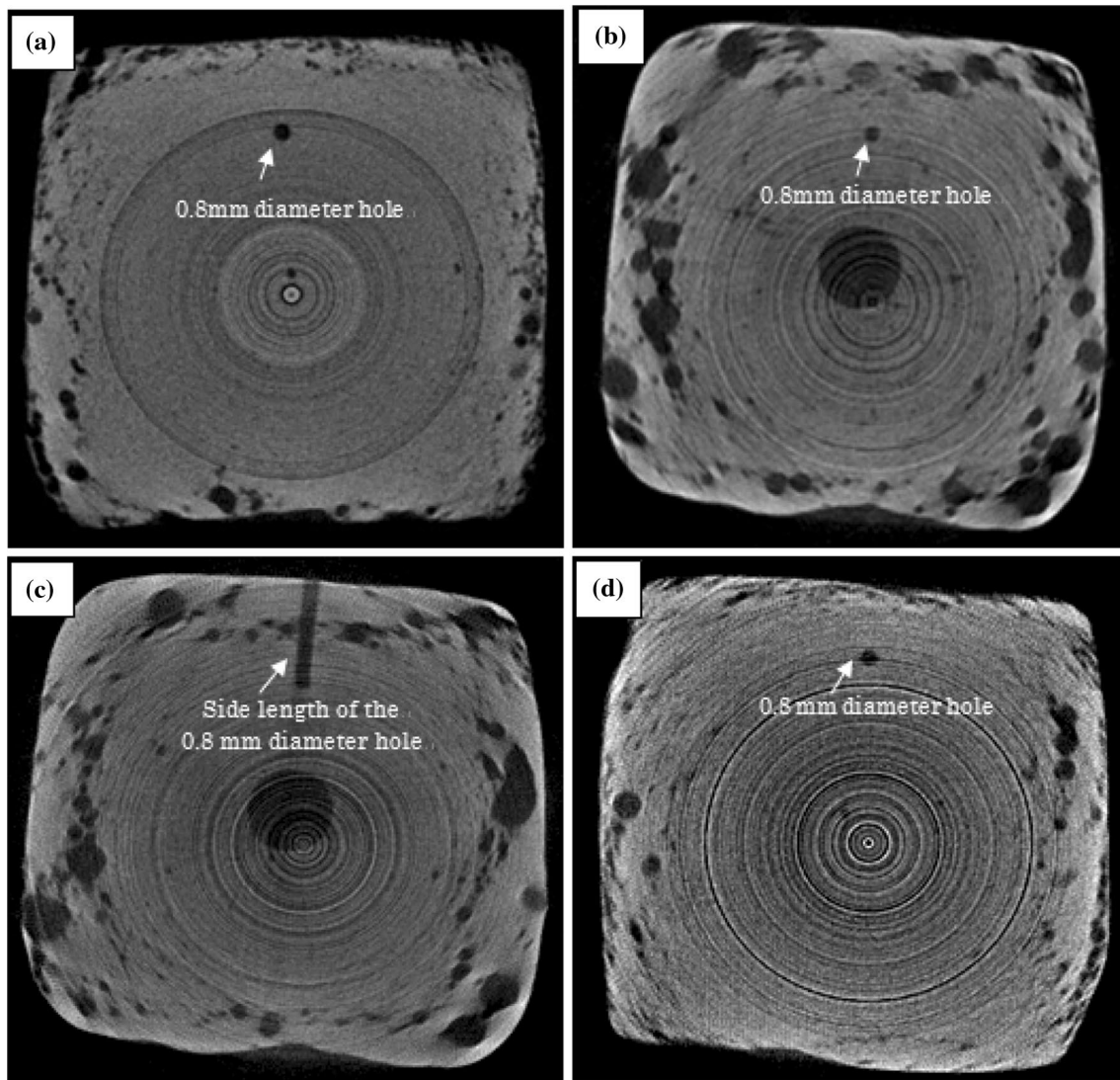


**Fig. 4** Some of the reconstructed CT slices images of the cuboid sample. **a** Top of the sample, **b**, **c** show the middle of the sample, the **d** bottom of the sample

shows the CT slice image, and (b), (c) shows the cross-sectional view of the selected yellow and blue color region by virtual sectioning, respectively. The actual value of the diameter and length of the holes should halve from CT's values shown in the above diagram due to the geometrically two times magnification of the object with experimental parameters. Hence the real value of the tiny holes will be approximately 0.8 mm in diameter and 1.10 cm and 0.6 cm in length. It clearly shows us that the calculated dimensional values from the CT images are identical to the values of the real object. Therefore, this virtual sectioning will be a great advantage for the observation of shapes and for calculating the dimensions of internal defects located anywhere within the objects. Further CT images produced by the FPD have shown the internal dimensions with precise accuracy.

Super Sealant Polymer Resin (P601) was used in the impregnating process for both Al-alloy cast samples, with the aim of carrying out non-destructive cone-beam XCT for identifying the impregnated resin and analyzing the defects before and after impregnation. Although many internal defects are present in the cast metal samples, the focus of our investigation is only on the holes that were created for this study. The high-resolution CdTe flat panel X-ray detector was outstanding in producing good color-contrast CT slice images, for classifying the resin parts, as shown in Figs. 8 and 9.

In this step, the frame rate of the FPD was increased from 10 to 50 fps, in order to achieve smoother and fewer artifacts and higher spatial resolution CT images. This enhanced its ability to differentiate between the two materials, as the

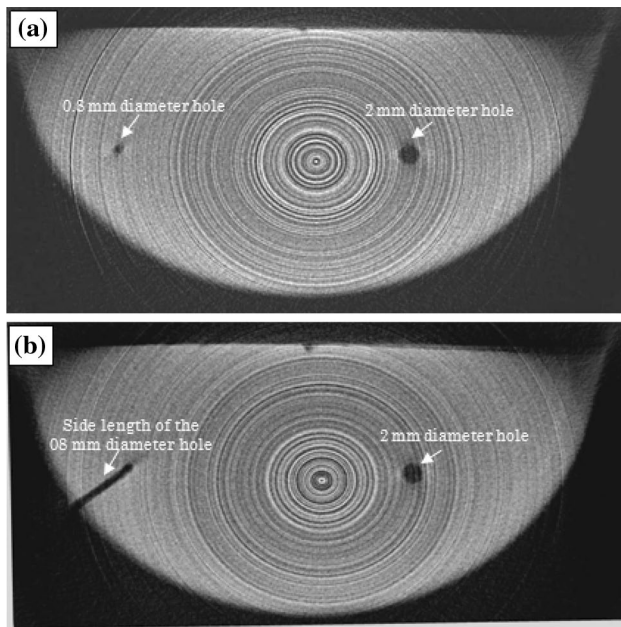


**Fig. 5** The reconstructed CT slice images of Al-alloys half-circle sample. **a** Top of the sample, **b** middle of the sample

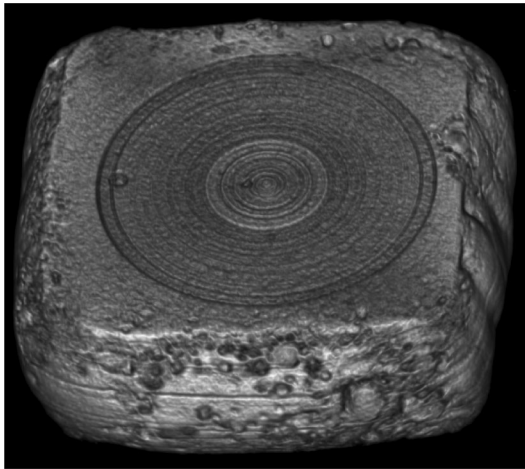


**Fig. 6** CT 3D image of the cuboid cast Al-alloys metal sample

number of projections in the CT increased from 720 to 3600. In the images of Figs. 8 and 9, gray value differences are visible between Al-alloys matrix, pores, and the two holes. The contrast of the impregnated regions could be visible with the different gray values, which are higher than the voids or surrounding air and less than the Al-alloys material. This deviation is due to the variation of X-ray attenuation for different materials. Voids and organic resin have lower X-ray absorption than Al-cast alloys. Hence, these XCT images reveal that some material should be existing in the holes after impregnation. It also shows that

the impregnated material does not homogeneously cover the two holes, and air bubbles have appeared in some places. The actual lengths of the impregnate material presence in the horizontal holes are around 5.50 mm for the cuboid and 6.28 mm for the half-circle sample. Figure 9b shows a cross-sectional CT image of the half-circle alloy sample with the two vertical holes, which are labeled as ‘A’ and ‘B.’ We conducted the impregnation treatment only for the hole ‘A,’ and it clearly shows the presence of some material inside the hole. However, the impregnate resin material has only existed in part of the hole, and the actual size is around 1.72 mm concerning the length of the hole 5 mm. This incomplete sealing would be due to the comparatively large size of the holes, properties of the impregnate resin such as viscosity, and conditions of the impregnation procedure (Temperature, Pressure, and Time). In this study, the impregnation process was carried out only for research purposes, and these results affirm proper practice that needs to be taken in the industrial impregnation process in order to achieve a better outcome. However, CT data of the Flat panel detector could not accurately recognize this material as the impregnation resin without proper quantitative analysis for material characterization.

### 3.2 Quantitative analysis of the cast Al-alloy samples

We executed the DXCT technique in order to determine the materials presented in the cuboid cast alloy sample based on their atomic numbers. The 64-pixel linear array photon-counting detector was used to take projection data of the sample after impregnation treatment and reconstructed CT images for two energy windows depicted as in Fig. 10.

These CT images show the different gray value contrast between the Al metal parts, voids, and the impregnating resin. The plotted attenuation coefficient values of the pixel in the selected region of high-energy window CT image also show clear evidence for the resin part, as depicted in Fig. 11.

$\mu$ CT comparison in four regions of the same image precisely provides the evidence for the presence of some material in which attenuation is higher than air (“B”) and less than the Al metal (“A,” “C”) in the impregnated region “D.” However, a careful study of the above diagram shows clearly that the existing material in the impregnated region (“D”) is not homogeneously spread and contains some low attenuation air bubbles. This situation can be minimized by improving the impregnation conditions within the industrial process. These outcomes also provide an excellent correlation with the results of the FPD study, though image quality has been slightly affected by ring artifacts.

Equation 1 of the DXCT technique was utilized to calculate effective atomic numbers of the selected regions of the XCT image in Fig. 10. The calculated effective atomic

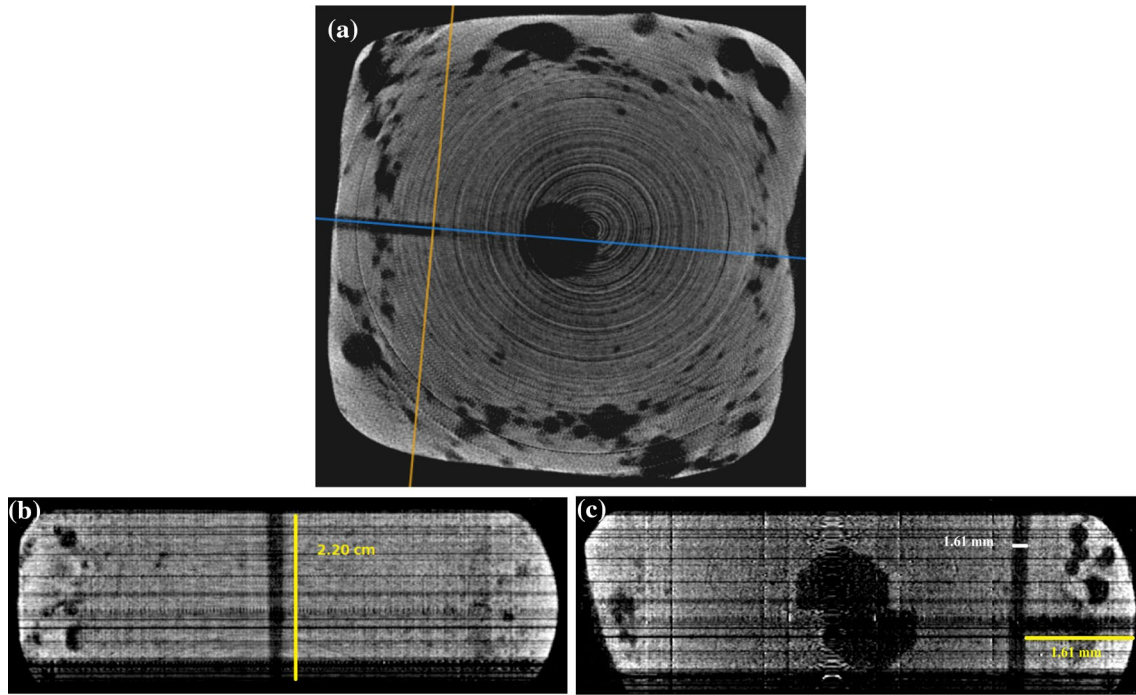


Fig. 7 Dimensions analysis of CT image of the cuboid cast alloys sample

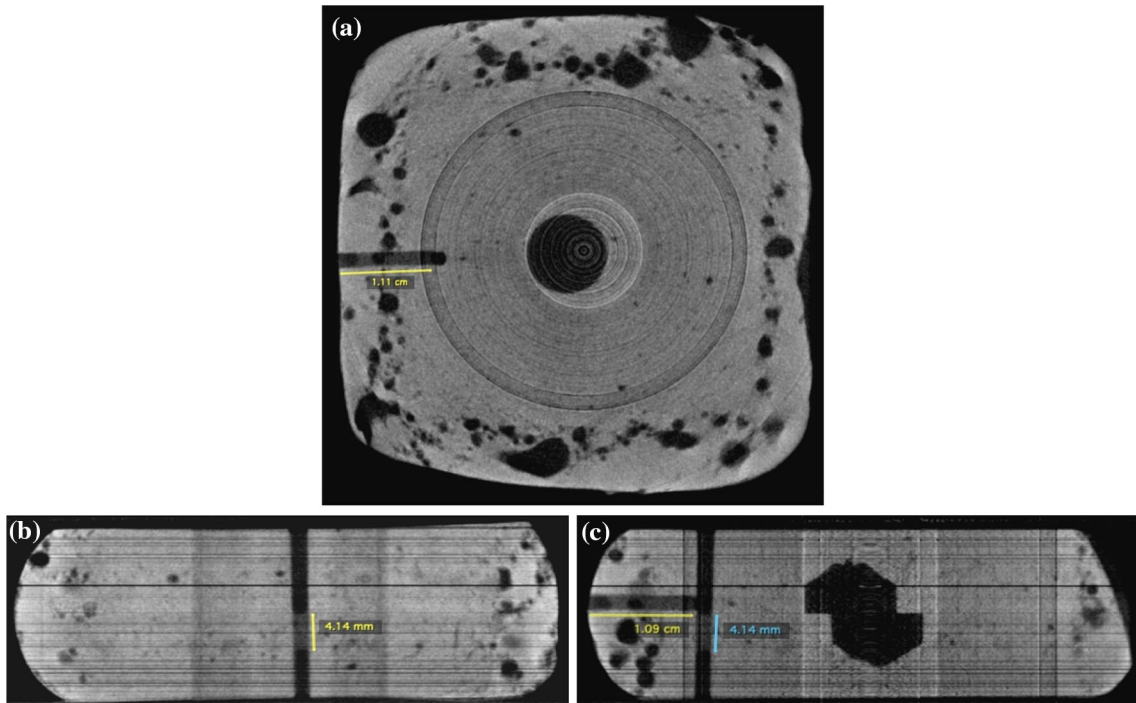
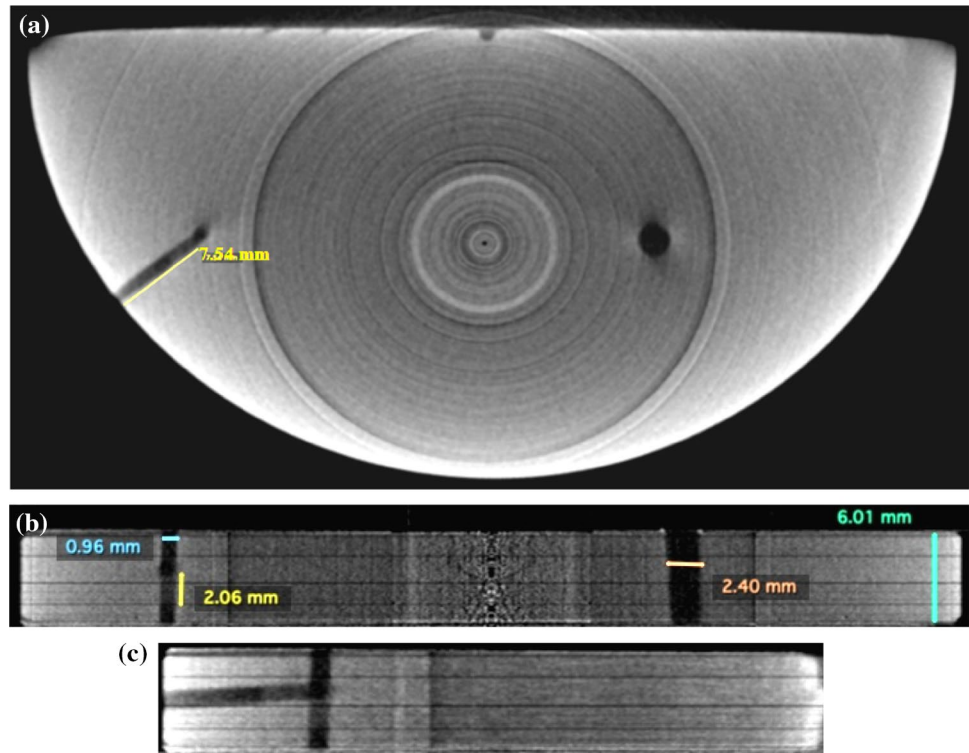


Fig. 8 CT images of the cuboid Al sample after impregnation. **a** A slice image, **b**, **c** cross-sectional images of the sample

numbers ( $Z_{exp}$ ) of the Al metal and the impregnated region material compared with their corresponding theoretical values ( $Z_{th}$ ). Also, a polymerized rigid sample of the same

impregnation resin (P601) was used to investigate the experimental effective atomic number, and all the results are listed in Table 1.

**Fig. 9** CT images of the half-circle Al sample after impregnation. **a** A slice image, **b, c** cross-sectional images of the sample



DXCT results of the above table provide clear evidence of the material characterizations based on effective atomic numbers. The error percentage of the effective atomic number of the Al die-casting alloys shows 14.92% for the atomic number of Al. This deviation is at the acceptable level because the die-casting alloys not only consist of Al metal, but they can also include some amount of other metals components, such as Si, Fe, Zn, and Sn. However, for the impregnation resin part of the Al cast metal, the error is 16.28%. In this calculation, we considered that the effective atomic number of methacrylate ( $C_6H_{10}O_3$ ) see Table 1 is the theoretical atomic number of the impregnation resin (P601). However, this assumption is not exactly accurate. Impregnation resin (P601) is a polymer compound that consists of hydroxyl ethyl methacrylate with other initiators and inhibitors. Therefore, the effective atomic number of the pure solid impregnation sample (P601) was calculated separately with the DXCT technique, and that value was 7.87. We then compared 7.87 with the experimental effective atomic number of the impregnated region material (7.64) in the die-casting alloy sample. Experimental conditions and the size of the selected region of both resin parts of the Al cast metal and the solid impregnation sample (P601) were kept constant for the atomic number calculation. These results show that the effective atomic number of the material presented in the impregnated region of the die-casting alloys was almost equal to the effective atomic number of the solid impregnation resin sample (P601) with a low error

percentage (2.92%). Hence, the DXCT results have confirmed that the present material in the impregnated region of the die-casting alloys is P601. This further supports the narrative that the dual-energy CT technique is regarded as a precise and efficient method for the nondestructive material characterization and dimensional analysis of cast alloys in the industry.

The conditions such as voltage, current of the X-ray source, scan resolution, physical parameters of the experimental setup, detector calibrations, and software handling are significant. With further improvements and proper controlling of these parameters, we would be able to achieve a higher degree of XCT accuracy.

## 4 Conclusion

In this study, we demonstrated that a high-resolution CdTe flat panel detector and photon counting line sensor could be effectively employed with a conventional microfocus X-ray tube system for the visualization of internal defects and material characterization in industrial cast Al-alloys. Specifically, a stack of 2D slice images of the cast alloys test pieces provides a specific aspect of the inside of the metal for fast defects inspections in the FPD analysis. The scan resolution and adequate magnification are vital for defect observation of the metal objects, and slow stepwise rotation ( $5^\circ/s$ ) of the sample with two times magnification was sufficient to



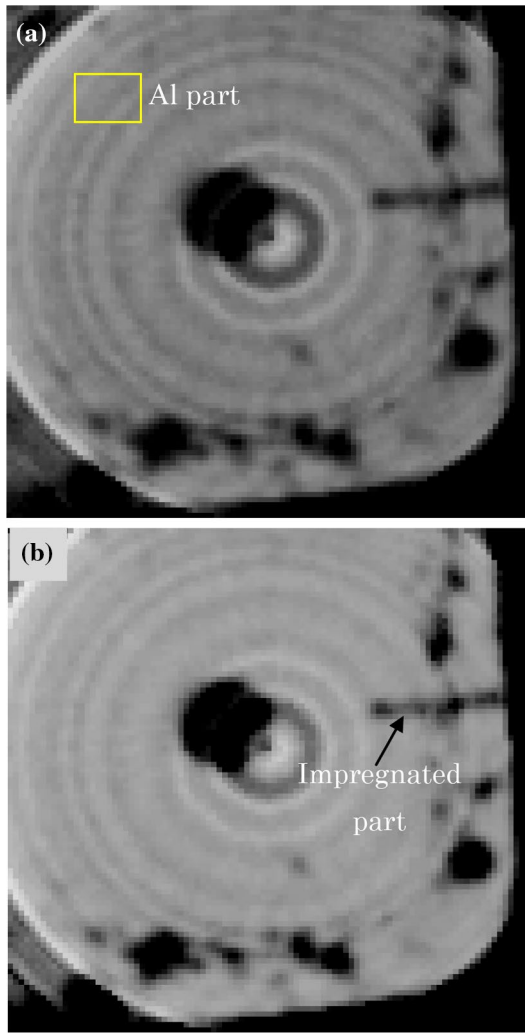


**Fig. 10** CT images of the cuboid Al-alloys sample. **a** Low energy and **b** high energy windows with the 64-pixel linear array photon-counting CdTe detector

produce appropriate CT images in our study. The spatial resolution of the CT images has improved dramatically with a higher number of projections. It was also possible to use virtual sectioning to create cross-sections of 3D CT images of metal samples in order to detect shapes and dimensions of the internal defects. Al-alloys partly shows a brighter region in the CT image due to high X-ray absorbing features and dark areas for voids.

The gray-value contrast in CT image of the FPD shows clear evidence for the presence of some material in the holes (0.8 diameters) after impregnation treatment, and it exhibits lower gray values than the alloys and higher than the voids due to X-ray attenuation differences. However, both alloy samples' CT images show inhomogeneities in the impregnated region, and the middle of the resin consists of some air bubbles. Also, the images display that the acrylic resin material was unable to seal the tiny holes completely. Therefore,

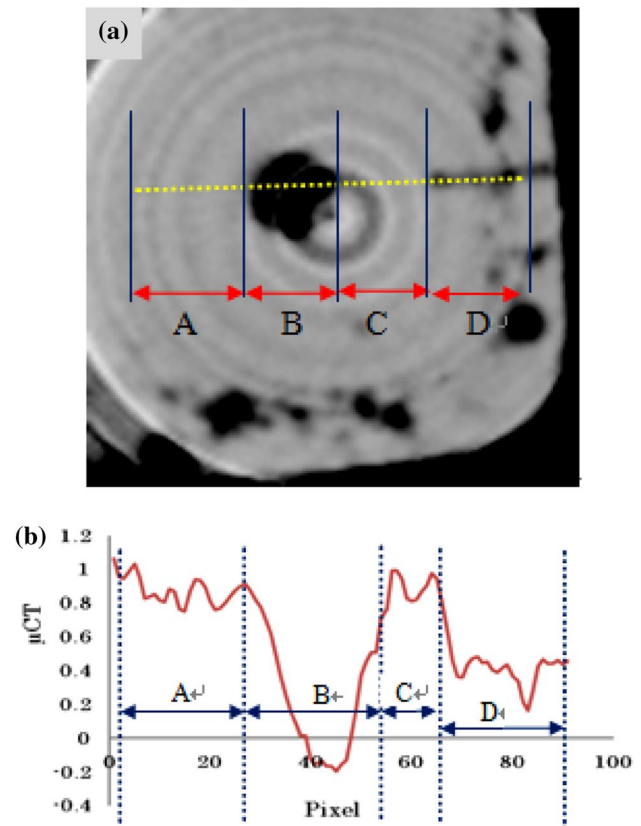


**Fig. 11** **a** High energy window CT image of the Al-alloys cuboid sample, **b**  $\mu$ CT values of pixels along the dotted line of the CT image

these FPD analyses with cone-beam geometry provide a great advantage to see the adequateness of the impregnation resin amount inside the defects of the cast alloys, and necessary steps can be considered to improve the quality of the industrial impregnation treatment. Also, the data provided by the DXCT analysis on the cuboid cast alloy samples by a 64-pixel, linear-array photon-counting line sensor shows a clear analogy with the results of FPD. Then, the effective atomic numbers based on the linear attenuation coefficient could be utilized to identify the impregnation resin material, which presents inside Al-cast alloys. The findings show that the experimental effective atomic number of the impregnated material present in the casted metal alloys is identical with the effective atomic number of the P601 super-sealant impregnate resin, with a 2.92% error percentage. Hence, the DXCT technique, with the aid of a fan beam collimator, is useful to material characterizations of the die casting alloys without destroying the sample.

Though some ring artifacts appeared in the CT images due to the miscalibrated or defective detector elements, this study's analysis of the defects is not significantly affected by them. A significant number of projections were obtained within 72S, and high-resolution CT slice images were generated in less than 10 min with the FPD. Therefore, an XCT

**Table 1** Comparisons of experimental results and theoretical data of the Cast Al-alloys cuboid sample with impregnation treatment

	$\mu\text{CT}$ (low energy)- $E_1$	$\mu\text{CT}$ (high energy)- $E_2$	$Z_{\text{exp}}$	$(Z_{\text{exp}}-Z_{\text{th}})/Z_{\text{th}}$ (%)
Al-die casting ( $Z_{\text{th}}=13$ )	0.80627	0.50404	14.94	14.92
Impregnation resin part of Al sample ( $Z_{\text{th}}=6.57$ )	0.36792	0.24227	7.64	16.28
Solid Impregnation sample (P 601) ( $Z_{\text{th}}=6.57$ )	0.22544	0.20940	7.87	19.78
Error percentage of the impregnation part of the Al sample to the P601 sample				$(7.64-7.87)/7.87$ 2.92%

with an advanced CdTe flat panel detector can be practically and effectively utilized for speedier defect inspections in the die-casting alloys industries.

**Acknowledgements** We wish to thank Koji Kobayashi for his technical support to the impregnation process. This research did not receive any specific grant from funding agencies in the public, commercial, or not-for-profit sectors.

**Author contributions** AB and HM carried out the experiment. AB wrote the manuscript with support from KK. AK and TA helped supervise the project. All authors discussed the results and contributed to the final manuscript.

## Compliance with ethical standards

**Conflict of interest** The authors declare that they have no competing interests.

## References

- Engelberger JF (1980) Die casting applications. Robotics in practice. Springer, Boston
- Casarotto F, Franke AJ, Franke R (2012) 6—High-pressure die-cast (HPDC) aluminium alloys for automotive applications. In: Rowe J (ed) Advanced materials in automotive engineering. Woodhead Publishing, Sawston, pp 109–149. <https://doi.org/10.1533/9780857095466.109>
- Benedyk JC (2010) Aluminium alloys for lightweight automotive structures, a volume in Woodhead Publishing series in composite science and engineering, materials, design and manufacturing for lightweight vehicles, pp 79–113
- Kaufman JG (2000) Introduction to aluminum alloys and tempers. ASM International, United States
- Fiorese E, Bonollo F, Timelli G et al (2015) Inter Metalcast 9:55. <https://doi.org/10.1007/BF03355602>
- Kanno T (1997) An Introduction to die casting technology. Nikkan-kogyo-sinbunsha, Tokyo, pp 227–247
- American Society for Testing of Materials ASTM E1742/E1742M, “Standard Practice for Radiography Examination”, Annual book of ASTM standards 2011 (03.03)
- Bossi RH, Georgeson GE (1992) Computed tomography analysis of castings, Boeing Defense and Space Group Seattle WA Aerospace and Electronics Div
- Baruchel J, Buffiere JY, Maire E, Merie P. and Peix (eds) G (2000). X-ray tomography in material science, 204; Hermes Paris Science publication, France
- Salvo L, Cloetens P, Maire E, Zabler S, Blandin JJ, Buffiere JY et al (2003) X-ray micro-tomography an attractive characterization technique in materials science. Nucl Instrum Meth Phys Res B 200:273–286
- Kastner J, Heim D, Salaberger D, Sauerwein Ch, Simon M (2006) Advanced applications of computed tomography by combination of different methods. In: Proceedings of 9th European Conference on Non-destructive Testing, Berlin. September 25–29, 2006
- Kastner J (2008) editor. Proceedings Industrielle Computertomografietagung; Wels, Austria, 26–27 February 2008
- Reinhart C (2008) Industrial computer tomography—A universal inspection tool. In: 17th world conference on nondestructive testing. 25–28 Oct 2008, Shanghai, China
- Ohno Y, Torikoshi M, Tsunoo T, Hyodo K (2005) Dual-energy x-ray CT with CdTe array and its extension. Nucl Instrum Methods Phys Res, Sect A 548:72–77. <https://doi.org/10.1016/j.nima.2005.03.069>
- Torikoshi M, Tsunoo T, Endo M, Noda K, Kumada M, Yamada S, Soga F, Hyodo K (2001) Design of synchrotron light source and its beamline dedicated to dual-energy x-ray computed tomography. J Biomed Opt 6(3):371–377
- Kastner J, Harrer B, Degischer HP (2011) High resolution cone beam X-ray computed tomography of 3D-microstructures of cast Al-alloys. Mater Charact 62:99–107
- Kan K, Imura Y, Morii H, Kobayashi K, Minemura T, Aoki T (2013) Application of photon-counting X-ray computed tomography to aluminum-casting inspection. World J Nucl Sci Technol 3:106–108
- Du Plessis A, Rossouw P (2015) X-ray computed tomography of a titanium aerospace investment casting. Case Stud Nondestruct Test Eval. <https://doi.org/10.1016/j.csndt.2015.03.001>
- Lauritsch G, Haerer WH (1998) A theoretical framework for filtered backprojection in tomosynthesis. Proc SPIE 3338:1127–1137
- Jackson DF, Hawkes DJ (1981) X-ray attenuation coefficients of elements and mixtures. Phys Rep 70(3):169–233
- Hawkes DJ, Jackson DF (1980) An accurate parametrisation of the x-ray attenuation coefficient. Phys Med Biol 25(6):1167–1171
- Zou W, Nakashima T, Onishi Y, Koike A, Shinomiya B, Morii H, Neo Y, Mimura H, Aoki T (2008) Atomic number and electron density measurement using a conventional X-Ray tube and a CdTe detector. Jpn J Appl Phys 47(9):7317–7323

**Publisher's Note** Springer Nature remains neutral with regard to jurisdictional claims in published maps and institutional affiliations.